Nonequilibrium Dynamics in Cuprate Superconductors using Transient Grating Spectroscopy

Peter Lu

under the direction of
Prof. Nuh Gedik
Fahad Mahmood
Massachusetts Institute of Technology

Research Science Institute
July 26, 2011

Abstract

Transient grating spectroscopy is an excellent method for probing the dynamics of quasiparticles in high-temperature superconductors, which are key to understanding the mechanism behind superconductivity in such materials. Femtosecond optical pulses provide time-resolved measurements of reflectivity. When combined with nonuniform excitation due to the diffraction grating, this technique can effectively separate diffusive quasiparticle dynamics from recombination. The Rothwarf-Taylor (RT) equations have, thus far, provided a successful framework to numerically analyze and understand transient grating measurements. However, most analyses rely on simplifications that result in analytic solutions, such as simple bimolecular recombination. Here, we directly numerically fit pump probe data to the RT equations and attempted to directly fit transient grating data to a generalization of the RT equations that included diffusion.

Summary

To have a material's resistance suddenly drop to zero is surprising enough, but to have this happen at approaching room temperature is even more so. Such a material, known as a high-temperature superconductor, does this spontaneously at a certain critical temperature. This property is caused by a macroscopic quantum phenomenon that is still not well understood. To get a better understanding of the dynamics and mechanism behind this, we used very short laser pulses to observe the change in reflectivity on the scale of picoseconds. This time-resolve spectroscopy allowed us to actually measure the way in which electrons in the material, knocked out of their superconducting state, return to equilibrium. In particular, the transient grating method was useful for separating different effects, such as diffusion, produced by the complicated way the laser pulse excites the electrons in the superconductor.

1 Introduction

Superconductors are materials that, due to quantum effects, allow electricity to flow free of resistance. Previous experiments have estimated that the damping of a current in a superconductor is on the order of 10^5 years, as opposed to fractions of a second in a normal conductor [1]. Because superconductivity is a macroscopic phenomenon caused by coherent quantum dynamics, it can not be fully understood using microscopic quantum theory or classical thermodynamics. Instead, superconductivity is best explained by a hybrid of these two theories.

1.1 BCS Theory

As a superconductor is cooled below its critical temperature, T_c, electrical resistance in the material experiences a sudden, sharp drop (Fig. 1(a)), which then causes the material to exhibit perfect diamagnetism (Fig. 1(b)). Conventional superconductors were not well understood until Bardeen, Cooper, and Schrieffer developed their theory, BCS Theory, in 1957 [1].

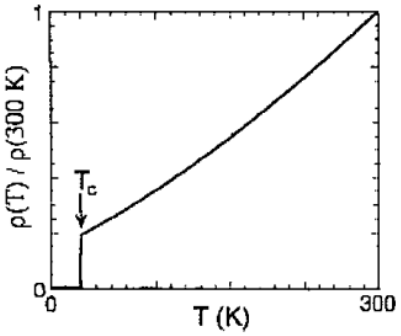

(a) *Critical temperature.* There is a sudden drop off in resistivity (ρ) at T_c in a superconductor.

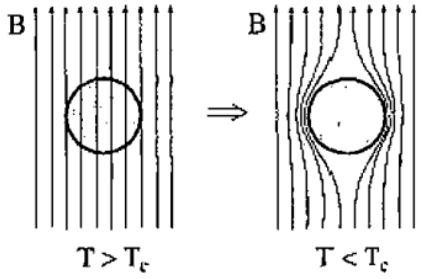

(b) *The Meissner effect.* A superconductor expels magnetic flux, causing magnetic field lines (B) to bend around it, due to perfect diamagnetism.

Figure 1: *Properties of superconductors.* These two properties are defining characteristics of superconductors [1].

BCS theory posits the mechanism behind superconductivity as quantum interactions between electrons and the crystal lattice of a superconductor. Quantized lattice vibrations, or phonons, are exchanged among the electrons in a superconductor. It is often more useful to characterize an electron in a conducting material as a so-called quasiparticle, which can have a different effective charge and mass to account for the electron-lattice interactions. At a sufficiently low temperature, these interactions will induce pairs of electrons, or quasiparticles, to bind together, forcing the two to have opposite spins and momenta. These couplings are known as Cooper pairs, in which two electrons, normally fermions (spin-1/2), together act as a composite boson (spin-0,1) [1]. Unlike the fermions that make up most of normal matter, bosons, such as the photons that make up light, can easily "pass through" each other, since multiple bosons can occupy the same quantum state. In the same way, Cooper pairs can easily flow through a superconductor.

1.2 High-Temperature Superconductors

Cooper pairs also possess long-range phase coherence. In a conventional metallic superconductor, this is achieved by the direct overlapping interactions of the Cooper pairs' wavefunctions, so the phase coherence is a byproduct of the electron pairing. However, in high-temperature superconductors, although the superconducting state does not occur until phase coherence is established at T_c, electron pairing can occur well above T_c. High-temperature superconductors become superconducting at temperatures that far exceed predicted theoretical limits [1]. Thus, BCS theory fails to explain the mechanism behind superconduction in these materials. Cuprates (copper oxides) were the first type of high-temperature superconductors discovered and remain a major focus of ongoing research [2]. In order to superconduct, cuprates must be doped, usually with "holes," the name given to the lack of an electron. These can be conceptually considered positive charge carriers. With doping, these unconventional superconductors have strong nonlinear electron-lattice interactions and thus have

much smaller Cooper pairs compared to conventional superconductors, so wavefunction coupling and coherence fail. Currently, it is believed that the high critical temperature of these superconductors is related to the anti-ferromagnetic structure of the CuO_2 planes of their crystal lattices, where the superconduction occurs. Spin fluctuations in the CuO_2 planes are believed to induce the necessary phase coherence for superconductivity [1]. Surprisingly, the strength of the electron-lattice interactions, which make these materials such good insulators at room temperature, is also the source of their high-temperature superconductivity. In addition, the nonlinearity of these interactions complicates theoretical modeling.

1.3 Pump Probe Spectroscopy

Current superconductor research involves a wide array of techniques. Advances in precision measurements allow us to directly image the surface of a cuprate using scanning tunneling microscopy, measure their optical absorption spectra, and detect minute magnetic fluctuations using neutron scattering [2].

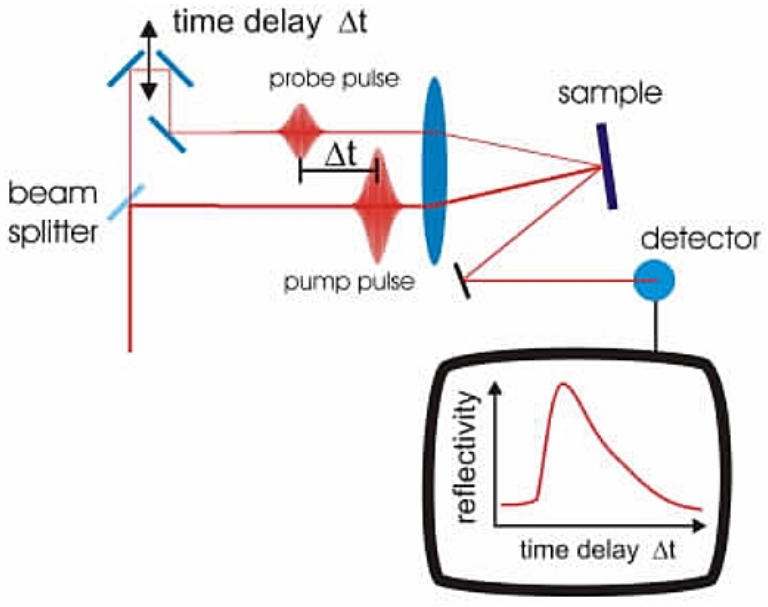

Figure 2: *Pump probe spectroscopy setup.* The time delay between the pump and probe beams allows time resolved measurements [3].

The development of pump probe spectroscopy, a form of ultrafast laser spectroscopy used to perform time-resolved reflectivity measurements on cuprates, is particularly relevant. In pump probe spectroscopy, two short pulses of laser light are directed at a sample cuprate, as shown in Fig. 2. The pump pulse excites and breaks up the Cooper pairs into quasiparticles. After a slight delay, the probe pulse arrives and is reflected off the excited surface, allowing the observation of quasiparticles recombining into Cooper pairs. This study focuses on a recent refinement of pump probe spectroscopy, called transient grating spectroscopy. This type of spectroscopy is similar to pump probe, but instead interferes two pump beams on the surface of the sample so that quasiparticle diffusion can be studied, yielding additional details about quasiparticle dynamics and further elucidating the physical properties of cuprates [4].

1.4 Analyzing Spectroscopy Data

Because ultrafast laser spectroscopy of high-temperature superconductors is inherently a nonlinear and nonequilibrium process, the complicated dynamics are not well understood. This means that there is no real theoretical framework to which data can be compared. Only phenomenological models exist, the most common being the Rothwarf-Taylor equations [5]. However, even this model is too difficult to analytically solve. Instead many limiting cases, which produce analytic solutions, have been studied and used [6]. This study argues that many of these limiting cases have invalid assumptions, and that pure numerical methods provide a better approach.

2 Materials and Methods

Pump probe spectroscopy measures the change in reflectivity, ΔR, of a probe beam reflected off of the sample cuprate as a function of time. Optimally doped $Bi_2Sr_2CaCu_2O_{8+x}$ (Bi-2212) was used in this study. Using the transient grating method, the data was then analyzed to determine two separate changes in magnitude (δ, η) and the phase (ϕ) of the reflection coefficient as a function of time [4]. Because the change in reflectivity is proportional to the change in quasiparticle density, this method offers a way to measure transient quasiparticle dynamics [7]. In addition, the transient grating method can isolate the diffusion from recombination and other processes involving quasiparticles, allowing them to be studied separately [2].

2.1 Experimental Apparatus

The experimental system, shown in Fig. 3, began with a diode-pumped Nd:Yag laser, which produced a continuous 514 nm beam at 4.5 W [4]. This was used to pump a Ti:Sapphire laser, which converted the beam into 60 fs pulses centered at 795 nm ($h\nu = 1.56$ eV) with a full fluence of 44 $\mu J/cm^2$ [8]. The pulses were passed through a pulse picker which reduced the frequency of the laser pulses from 80 MHz to 1.6 MHz to avoid continuously heating the sample. A polarizing beam splitter (PBS) then separated the beam into a stronger pump beam and weaker probe beam. The probe was sent through a delay line, which ensured that the probe reached the sample after the pump. The P-polarized pump beam was first sent through a photoelastic modulator (PEM), which sinusoidally modulated the intensity of the beam, used later for lock-in amplification. The pump was then passed through neutral density (ND) filters that allowed the pulse fluence to be varied. Finally, a vibrating motor (Clark-MXR ODL-150) oscillated a mirror that modulated the path length of the pump beam. The delay between the pump beam excitation and the probe beam measurement can be altered

to measure the reflectivity at different times after the initial excitation. The vibrating motor allowed the delay between the pump and the probe to be quickly and continuously changed so that, in one sweep, the reflectivity at all times within the range of the motor's oscillation could be measured [4].

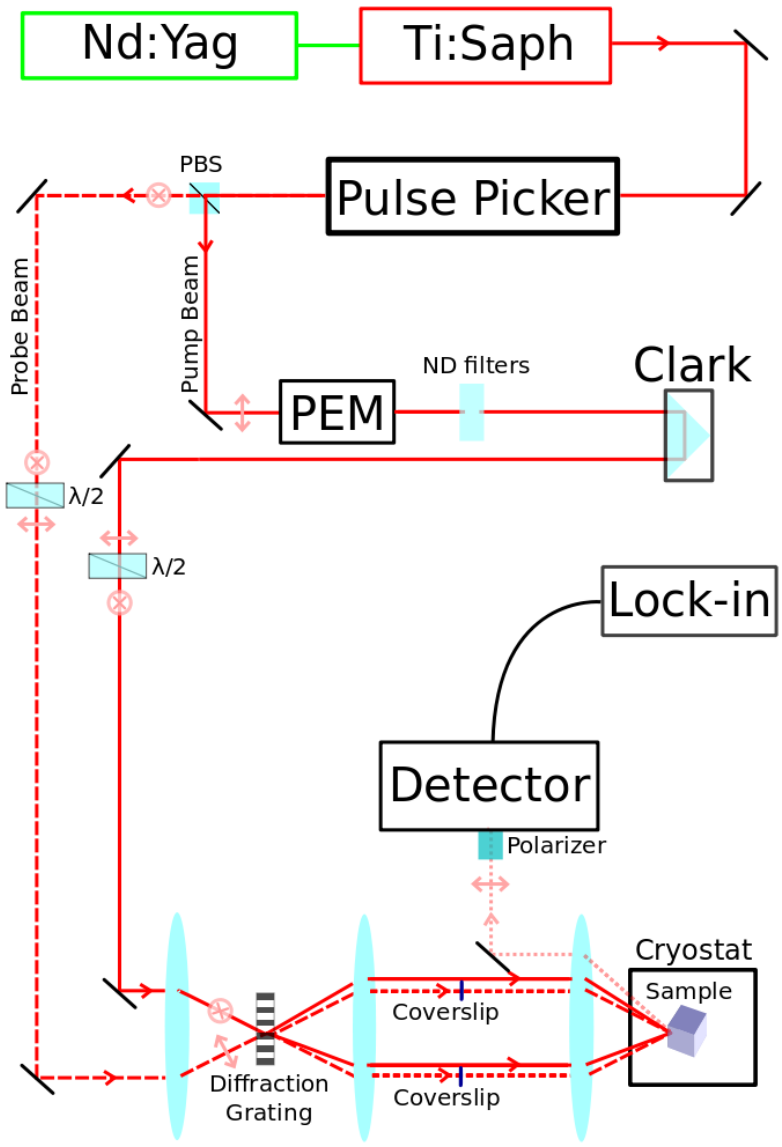

Figure 3: *Schematic of the transient grating apparatus.*

Before hitting the sample, the pump and the probe beams were sent through a diffraction grating, with spacing λ_g, that split each beam into two (taking only the first order diffraction), resulting in four beams in a rectangular arrangement known as the boxcar geometry (Fig. 4). The two probe beams were then passed through coverslips, which could be adjusted to vary the phase between the beams. This set of four beams was then focused onto the sample, and this particular geometry allowed the two diffracted pump beams to interfere on the surface of the sample, generating a grating of the same spacing (λ_g). In addition, the boxcar geometry ensured that the diffracted portion of one probe beam was always collinear with the specular reflection of the other, forming a local oscillator (LO). The two probe beams were interchangeable, so either could be the local oscillator. Therefore, we could measure two different probe signals, a top arm and a bottom arm, which were crucial for calibration [9]. The nonuniformity of pump beam excitation made it possible to study quasiparticle diffusion as well as recombination. Before the probe beam entered the detector, a photodiode, it was passed through a polarizer filter so the the S-polarized pump light did not enter the filter and add noise to the signal. The sample of Bi-2212 was first mechanically exfoliated to obtain a flat and clean crystal layer. It was then held in a cryostat at approximately 5 K and 10^{-7} torr to maintain superconductivity and avoid contamination that would alter the reflective properties of the cuprate, skewing spectroscopy data.

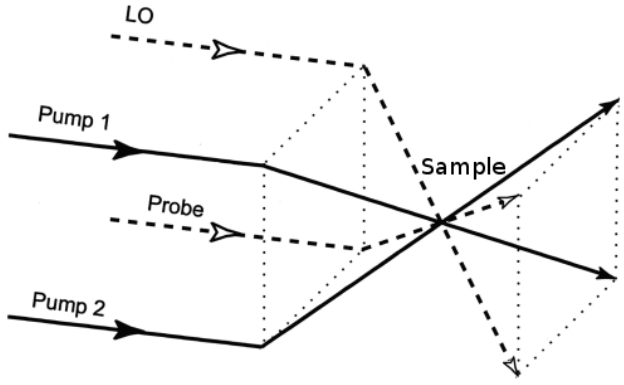

Figure 4: *Schematic of the boxcar geometry.* The sample is at the intersection of the beams [9].

2.2 Data Analysis

In order to interpret transient grating spectroscopy, significant data analysis and processing was required. In particular, the diffracted and refracted portions of the detected beam must be separated in order to measure diffusion.

2.2.1 Signal Processing

The signal from the detector is a measurement of the intensity (I_D) of the beam swept over time by the vibrating motor. The intensity at the detector is a combination of the reflected and diffracted probe beams [10]:

$$\begin{aligned} I_D &= I_0 + \Delta I_{1/2} \\ &= |E_P r_0|^2 + 2|E_P r_0|^2 \left[|\delta| \cos\phi + |\eta| \cos(\theta \mp \phi)\right], \end{aligned} \tag{1}$$

where E_P is the electric field of the probe beam, r_0 is the equilibrium reflection coefficient, δ is the change in the reflection coefficient due to the reflected beam, η is the change in the reflection coefficient due to the diffracted beam, ϕ is the phase of the reflection coefficient, and θ is the phase difference between the two probe beams. A lock-in amplifier was used to lock into the intensity modulation of the PEM, and separate the first and second terms of (1). This gives the fractional change in reflectivity ($\frac{\Delta R}{R}$) for the top and bottom arms [10]:

$$\frac{\Delta R}{R} = \frac{\Delta I_{1/2}}{I_0} = |\delta| \cos\phi + |\eta| \cos(\theta \mp \phi). \tag{2}$$

For calibration, we varied the phase, θ, between the two probe beams by varying the coverslip angle, ψ, since ψ is a linear function of θ. Using both the top and bottom arms (2), we found the two angles ψ_1 and ψ_3 at which $\frac{\Delta R}{R} = \frac{\Delta I_1}{I_0} = \frac{\Delta I_2}{I_0}$, or when $\theta = 0$ or π (i.e. the intersection of the top and bottom arms as a function of ψ, shown in Fig. 5). Since it is a

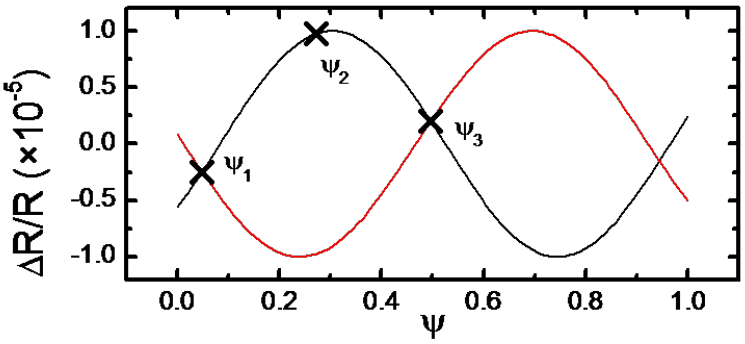

Figure 5: *Phase calibration.* ψ_1, ψ_2, and ψ_3 are found by varying ψ for the top and bottom arms and marking intersection points that correspond $\theta = 0$ and π. The ψ_2 is the average of ψ_1 and ψ_3, corresponding to $\theta = \frac{\pi}{2}$.

linear function, the linear combination $\psi_2 = \frac{\psi_1+\psi_3}{2}$ can be found at $\theta = \frac{\pi}{2}$. Using on the order of 10^3 averaged measurements of $\frac{\Delta I_{1/2}}{I_0}$ at the coverslip angles ψ_1, ψ_2, and ψ_3 (corresponding to $\theta = 0$, $\frac{\pi}{2}$, and π), we could produce three equations from Eq. 2 and solve for the three time-dependent variables $|\delta|$,$|\eta|$, and ϕ [10]:

$$\begin{aligned}
\frac{\Delta I_{\psi_1}}{I_0} &= |\delta| \cos\phi + |\eta| \cos\phi, \\
\frac{\Delta I_{\psi_2}}{I_0} &= |\delta| \cos\phi + |\eta| \sin\phi, \\
\frac{\Delta I_{\psi_3}}{I_0} &= |\delta| \cos\phi - |\eta| \cos\phi.
\end{aligned} \tag{3}$$

Due to the extensive data processing necessary in the transient grating method, we also took pump probe data (simply by removing the diffraction grating from the setup) in order to first obtain diffusion-independent parameters. With pump probe spectroscopy, we could only measure the average effect on the reflectivity, $\left(\frac{\Delta R}{R}\right)_{avg}$:

$$\left(\frac{\Delta R}{R}\right)_{avg} = |\delta| \cos\phi. \tag{4}$$

2.2.2 Fitting and Parameter Extraction

The pump probe data was first fit to the Rothwarf-Taylor (RT) differential equations (Eq. 5), which have been found to accurately model quasiparticle dynamics in superconductors, but do not take into account diffusion. The RT equations assume that a binding phonon ($E = 2\Delta$) is released when a Cooper pair dissociates and captured when a Cooper pair forms. Thus, the RT model uses a pair of coupled differential equations with two number density variables: n, the quasiparticle number density, and N, the binding phonon number density. The three main processes, illustrated in Fig. 6, are the bimolecular recombination rate of quasiparticles into Cooper pairs (βn), the rate at which Cooper pairs dissociates into quasiparticles (γ_{pc}), and the rate at which binding phonons escape the system (γ_{esc}) [8].

$$\begin{aligned} \frac{dn}{dt} &= -\beta n^2 + 2\gamma_{pc} N + I_n \\ \frac{dN}{dt} &= \frac{\beta}{2} n^2 - \gamma_{pc} N - \gamma_{esc}(N - N_{eq}) + I_N \end{aligned} \tag{5}$$

N_{eq} is the equilibrium phonon number density, and I_n, I_N are external generation rates for quasiparticles and phonons, respectively.

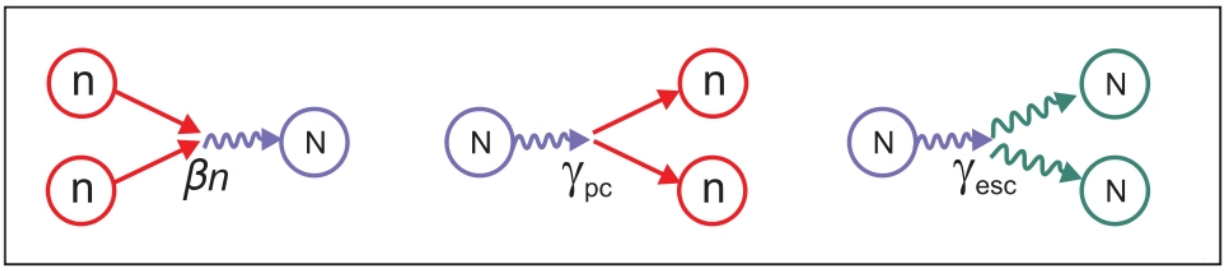

Figure 6: *Rothwarf-Taylor model.* βn is the rate at which two quasiparticles recombine, releasing a binding phonon. γ_{pc} is the rate at which a phonon break apart a Cooper pair, creating two quasiparticles. γ_{esc} is the rate at which phonons escape from the system, returning it to thermal equilibrium [8].

At low pump fluences, the thermal density of quasiparticles becomes relevant, meaning that a photoinduced quasiparticle can recombine with another photoinduced quasiparticle

(βn_{ph}) or a thermal quasiparticle (βn_{th}). Thus, the total density of quasiparticles can be written as $n = n_{ph} + n_{th}$ and total density of binding phonons as $N = N_{ph} + N_{eq}$. At thermal equilibrium, the rate of dissociation and creation Cooper pairs are equal ($2N_{eq}\gamma_{pc} = \beta n_{th}^2$), so Eq. 5 reduces to Eq. 6, assuming thermal densities are constant in time ($\frac{dn_{th}}{dt} = \frac{dN_{eq}}{dt} = 0$). Thus, $\gamma_{th} = \beta n_{th}$ is the characteristic rate of thermal quasiparticle recombination.

$$\begin{aligned}\frac{dn_{ph}}{dt} &= -\beta n_{ph}^2 - 2\beta n_{ph} n_{th} + 2\gamma_{pc} N_{ph} + I_n \\ \frac{dN_{ph}}{dt} &= \frac{\beta}{2} n_{ph}^2 + \beta n_{ph} n_{th} - \gamma_{pc} N_{ph} - \gamma_{esc} N_{ph} + I_N \end{aligned} \tag{6}$$

The pump probe signal $|\delta| \cos\phi$, defined in Eq. 4, was fit to the photoinduced quasiparticle number density (n_{ph}) over times approximately 0.5 ps after the beginning of the signal to avoid the initial pump pulse. This allowed us to make the assumption that $I_n = I_N = 0$. By fitting multiple fluences at once, we could accurately extract the parameters β, γ_{pc}, γ_{esc}, and n_{th}. Then, by adding diffusion terms, the RT equations could be generalized in order to include spatial effects (Eq. 7). This added two new parameters, the diffusion coefficients for quasiparticles (D_n) and phonons (D_N).

$$\begin{aligned}\frac{\partial n_{ph}}{\partial t} &= D_n \frac{\partial^2 n_{ph}}{\partial x^2} - \beta n_{ph}^2 - 2\beta n_{ph} n_{th} + 2\gamma_{pc} N_{ph} \\ \frac{\partial N_{ph}}{\partial t} &= D_N \frac{\partial^2 N_{ph}}{\partial x^2} + \frac{\beta}{2} n_{ph}^2 + \beta n_{ph} n_{th} - \gamma_{pc} N_{ph} - \gamma_{esc} N_{ph} \end{aligned} \tag{7}$$

Spatially, sinusoidal initial conditions with wavelength equal to the grating spacing λ_g and periodic boundary conditions were assumed when numerically solving Eqs. 7. Using the parameters extracted by fitting the pump probe data, these two diffusion coefficients were determined by fitting the transient grating data. The calculated values for $|\delta| \cos\phi$ and $2|\eta|$ were fit to the spatial average of $n_{ph}(x,t)$ and the peak-to-peak modulation in $n_{ph}(x,t)$, respectively. MATLAB was used to numerically integrate the differential equations while

using the trust-region reflective algorithm for nonlinear least-square optimization to extract parameters. The differential equation solutions were offset by a constant to take into account reflectivity changes due to other effects, such as the heating of the sample.

3 Results

The following data were taken from the same sample of Bi-2212. To avoid the initial pump pulse, the fits start from ≈ 0.5 ps after the beginning of the signal. Two separate runs of pump probe data were analyzed, resulting in the sets of parameters listed in Table 1. Fluences 2.2, 1.4, 0.70, and 0.44 μJ/cm^2 in each run were fit to the same parameters (Fig. 7).

	γ_{pc} (ps^{-1})	γ_{esc} (ps^{-1})	β (n^{-1} ps^{-1})	n_{th} (n)	γ_{th} (ps^{-1})
Run 1	0.049 ± 0.007	2.48 ± 0.07	0.544 ± 0.003	0.0268 ± 0.0002	0.0146 ± 0.0001
Run 2	0.069 ± 0.002	2.18 ± 0.06	0.454 ± 0.002	0.0394 ± 0.0002	0.0179 ± 0.0001

Table 1: *Pump probe fit parameters.* These parameters are from two separate runs of pump probe data fit to RT. Error bars reflect the range of parameter values obtained when varying the initial point of the fit over 0.2 ps. The unit "n" refers to an arbitrary number density unit.

The shoulder at around 10 ps, probably due to a reflection of the pump pulse, is accounted for with a small Gaussian source with standard deviation $\sigma < 0.5$ ps. Using the parameters in Table 1 as a starting point, transient grating data with a grating spacing of 5 μm were fit to Eqs. 7, fitting fluences 2.2, 1.4, and 0.70 μJ/cm^2 simultaneously. The resulting fit parameters are shown in Table 2. Although a good fit can be found (Fig. 8), the diffusion terms in the RT equations are extremely unstable during the fitting process and depend on constraints, so only the correct order of magnitude can be confirmed.

D_n (cm^2/s)	D_N (mm^2/s)	γ_{pc} (ps^{-1})	γ_{esc} (ps^{-1})	β (n^{-1} ps^{-1})	n_{th} (n)	γ_{th} (ps^{-1})
19.9	1.32	0.079	1.01	0.440	0.0200	0.0201

Table 2: *Transient grating fit parameters.* These parameters are for transient grating data fit to RT with diffusion terms. The unit "n" refers to an arbitrary number density unit.

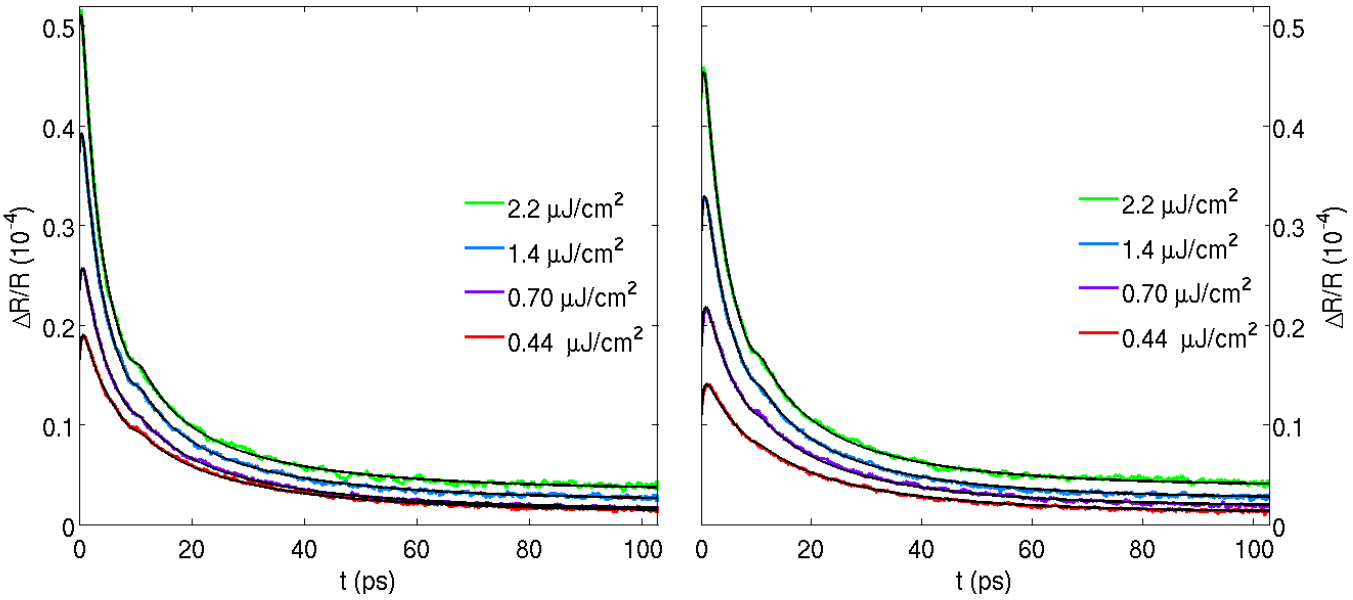

(a) *Run 1 data and fits.* (b) *Run 2 data and fits.*

Figure 7: *Pump probe data and fits.* Colored lines are pump probe reflectivity data. Black lines are the fits using the parameters in Table 1. Legend labels are in order from top to bottom.

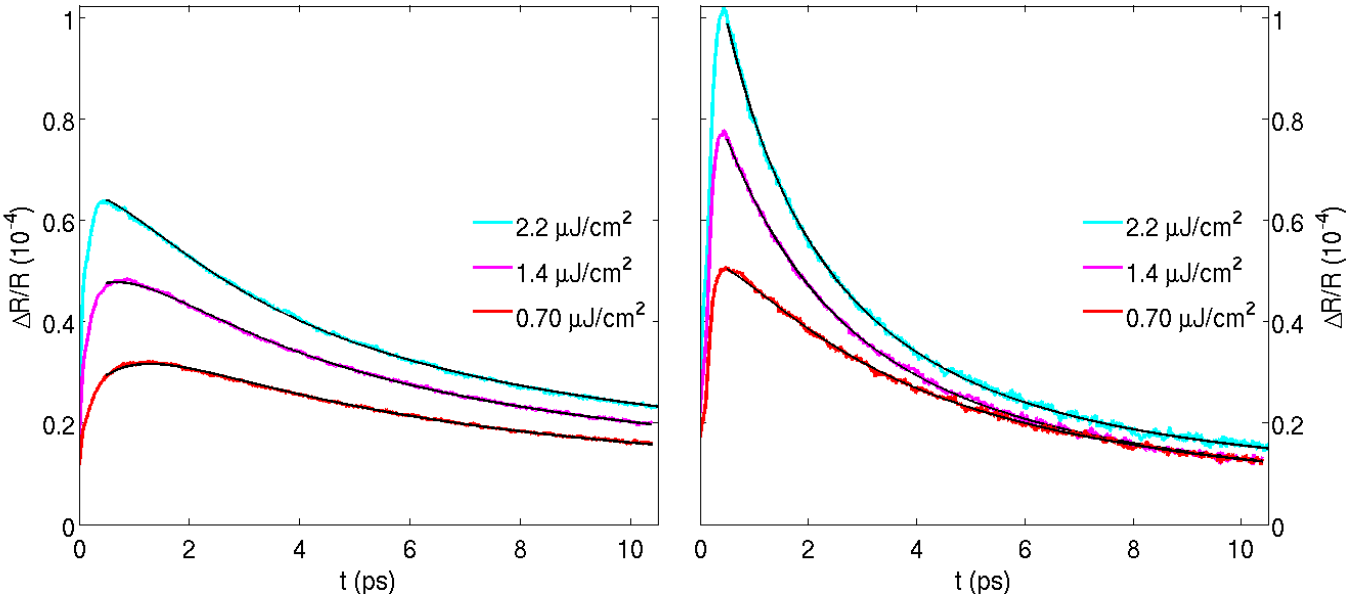

(a) $|\delta|\cos\phi$ *data and fits.* (b) $2|\eta|$ *data and fits.*

Figure 8: *Transient grating data and fits.* Colored lines are $|\delta|\cos\phi$ and $2|\eta|$ calculated from raw data. Black lines are the fits using the Table 2 parameters. Legend labels are in order from top to bottom.

4 Discussion

As expected, the RT equations can be fit well to the pump probe data. Differences between the two runs can be attributed to condensation and other uncontrolled changes to the cuprate sample's surface due to the cooling process, since the sample is recooled to 5 K for each run, which take place over two separate days. The addition of the diffusion terms make it necessary to numerically solve a set of partial differential equations. This requires additional assumptions, including uniform sinusoidal initial conditions that allow the use of periodic boundary conditions, and additional parameters. As a result, these complications may contribute to the fitting instability. However, our diffusion fit provides diffusion coefficients of the right order of magnitude: $D_n = 19.9$ cm^2/s $\sim$ 20–24 cm^2/s from diffusion measurements of YBCO [10], and $D_N = 1.32$ mm^2/s is on the order of thermal diffusion. Perhaps additional data, with varied fluences and grating spacings, would yield more consistent results. It is also possible that, since RT is only a phenomenological model, Eq. 7 is an invalid generalization to include diffusion.

Very few attempts to obtain a direct fit to the RT equations, which are not analytically solvable, have been made. Most make simplifying assumptions that make the equations analytically tractable. In particular, assuming $\gamma_{pc} \ll \beta n$ results in a simple bimolecular solution [4], and assuming $\frac{\gamma_{esc}}{\gamma_{pc}} \ll 1$ produces a conservation law and another analytic solution [6]. Some groups have even chosen to fit directly to a linear combination of exponentials, usually two, with no theoretical basis [11]. The analyses in this study indicate that many of these assumptions about the relative parameter sizes fail in the measurement range. Numerical solutions can comprehensively encompass the dynamics in RT and produce consistent results that match pump probe data.

5 Conclusion

A phenomenological model often fails to fully describe data, and simplifications based on poor assumptions will only make this worse. By numerically fitting pump probe spectroscopy data from the cuprate Bi-2212 to the RT equations, we were able to obtain very precise parameters. Although we were not able to extract diffusion coefficients with great precision, our pump probe fits show that using direct numerical methods to find fit parameters remains a very promising method for obtaining results unrestricted by simplifying assumptions.

6 Acknowledgments

I would like to thank my mentor, Professor Nuh Gedik, graduate student Fahad Mahmood and postdoctoral fellow Darius Torchinsky at the Massachusetts Institute of Technology for giving me the opportunity to work in their lab and guiding me along the way. In addition, I want to thank Dr. Jenny Senodova, Zachary Wissner-Gross, Jodi Balfe, and Kevin Burdge for editing this paper and all of the Research Science Institute (RSI) staff for providing me with advice and support. Finally, I thank the Center for Excellence in Education, SAP AG, Mr. and Mrs. Edward Noonan, and Dr. Sapan Shah for making this project possible.

References

[1] A. Mourachkine, *High-Temperature Superconductivity in Cuprates* (Kluwer Academic Publishers, Dordrecht, 2002).

[2] B. Keimer, Science **300**, 1381 (2003).

[3] A. Kolitsch, *Femtosecond spectroscopy of new materials* (2011), URL `http://www.hzdr.de/db/Cms?pNid=116&pOid=11985`.

[4] N. Gedik, Ph.D. thesis, Lawrence Berkeley National Laboratory (2004).

[5] A. Rothwarf and B. Taylor, Phys. Rev. Lett. **19**, 27 (1967).

[6] V. Kabanov, J. Demsar, and D. Mihailovic, Phys. Rev. Lett. **95**, 147002 (2005).

[7] G. Segre, N. Gedik, J. Orenstein, D. Bonn, R. Liang, and W. Hardy, Phys. Rev. Lett. **88**, 137001 (2002).

[8] D. Torchinsky, G. Chen, J. Luo, N. Wang, and N. Gedik, Phys. Rev. Lett. **105**, 27005 (2010).

[9] N. Gedik and J. Orenstein, Opt. Lett. **29**, 2109 (2004).

[10] N. Gedik, J. Orenstein, R. Liang, D. Bonn, and W. Hardy, Science **300**, 1410 (2003).

[11] P. Kusar, J. Demsar, D. Mihailovic, and S. Sugai, Phys. Rev. B **72**, 014544 (2005).